https://doi.org/10.5194/essd-2026-29
Preprint. Discussion started: 7 April 2026

Open Access Earth System Science Data Discussions

Fusing Local and Regional Datasets to Develop a Composite Land Cover Product Across High Latitudes

Valeria Briones[1], Hélène Genet[2], Elchin E. Jafarov[1], Brendan M. Rogers[1], Jennifer D.Watts[1], Anna-Maria Virkkala [1] Annett Bartsch[3], Benjamin C. Maglio[2], Joshua M. Rady[1], Susan M. Natali[1]

[1] Woodwell Climate Research Center, Falmouth, MA, 02540, USA
[2] Institute of Arctic Biology, University of Alaska Fairbanks, AK 99775 Fairbanks, USA
[3] b.geos, Industriestrasse 1, 2100 Korneuburg, Austria

Correspondence to: Elchin E. Jafarov (ejafarov@woodwellclimate.org)

Abstract

Rapid warming across the Arctic is the primary driver of widespread permafrost thaw, with far-reaching consequences for local ecosystem resilience, the regional carbon budget, and the global climate system. Because permafrost characteristics and vulnerability are tightly linked to land cover, particularly vegetation type and surface properties, understanding these dynamics requires accurate and detailed land cover information. Spatial variation in vegetation cover influences energy balance, snow insulation, and soil moisture, factors that directly affect permafrost stability. Consequently, high-resolution land cover products are essential for assessing the ecological impacts of permafrost thaw and for improving the representation of permafrost-related processes in predictive models. However, many global land cover datasets fail to capture the spatial heterogeneity and fine-scale ecological features that influence permafrost dynamics, while more detailed regional products often lack coverage across broader, continental extents. This gap presents a challenge for large-scale assessments of permafrost vulnerability under accelerating climate change.

To create a spatially cohesive land cover map that accurately represents the distribution of ecosystems across the Arctic-Boreal region, we integrated existing global and regional land cover datasets using a workflow including machine learning techniques. This approach seamlessly combines diverse data sources, enhancing representation and accuracy. The resulting map represents high-latitude land cover types at a 1km spatial resolution, better capturing the spatial heterogeneity of the landscape compared to coarser resolution land surface products, with a total of 35 land cover classes, including 20 forest types (e.g., Larch, Birch, Mixed forests), 6 shrubland classes, and wetlands subdivided into bog, fen, and marsh. To achieve this, we used a global land cover map, the European Space Agency Climate Change Initiative Land Cover data (ESA CCI-LC), as the base map and integrated regional maps across the circumpolar region with finer-resolution land cover information to capture the diversity of land cover types. This approach ensured consistent classification across geopolitical boundaries, while incorporating representative vegetation communities at a region-specific level. Here we documented a workflow used to produce a harmonized circumpolar land cover dataset at 1 km² resolution, encompassing the time period 2000-2023. The hybrid land cover is an open-source product https://doi.org/10.5281/zenodo.17968808 (Briones et al 2025).

1. Introduction

High-latitude regions play a critical role in the global climate system because of the intricate interplay of biophysical and biogeochemical processes that regulate terrestrial carbon and energy balances (Heimann & Reichstein, 2008). Climate change is reshaping these processes, contributing positive feedbacks that amplify global warming (Intergovernmental Panel on Climate Change, 2022). Warming temperatures and altered precipitation regimes are intensifying disturbance dynamics, including permafrost thaw and wildfires, thereby increasing

https://doi.org/10.5194/essd-2026-29
Preprint. Discussion started: 7 April 2026

ecosystem vulnerability to state change (Johnstone et al., 2016; Schuur et al., 2022). These climate–disturbance interactions are driving vegetation shifts that modulate ecosystem structure and function, affecting both above- and belowground carbon cycling (Poulter et al., 2015) and surface energy exchange (Oehri et al., 2022; Thompson et al., 2004). For example, increases in tree and shrub density in the Arctic–Boreal Zone (ABZ) decrease surface albedo, accelerate regional warming (Betts, 2000; Bonfils et al., 2012; Miller & Smith, 2012), and alter snow, nitrogen, and permafrost dynamics (Elmendorf et al., 2012; Tape et al., 2006; J. A. Wang et al., 2020; Zhang et al., 2013). Understanding and projecting the consequences of these changes requires accurate characterization of vegetation and land cover (Balshi et al., 2009; Mack et al., 2021; Virkkala et al., 2018; Horvath et al., 2021; Kåresdotter et al., 2021).

Land cover integrates the effects of climate, disturbance, landform, and soil characteristics, and is therefore a critical driver of the spatial heterogeneity of ecological processes. Accurate land cover representation is particularly important in high-latitude systems where vegetation strongly influences ecosystem vulnerability and climate feedbacks. Detailed depictions of vegetation composition are needed to improve projections of carbon and energy fluxes, permafrost stability, and disturbance impacts.

Remote sensing has become the primary tool for generating such information, leading to the development of both global and regional products (Joshi et al., 2016; Rogan & Chen, 2004). However, these mapping efforts vary widely in spatial resolution and classification detail, creating trade-offs that limit their ability to consistently represent vegetation diversity across the circumpolar Arctic–Boreal Zone. Global products offer broad spatial coverage but typically rely on coarse, generalized classes that fail to capture the heterogeneity of Arctic and Boreal systems. In contrast, regional products provide finer resolution and more detailed vegetation classes, but are limited in spatial extent. This trade-off complicates large-scale ecological investigations requiring both ecological detail and cohesive circumpolar coverage.

Tundra vegetation plays a critical role in modulating surface energy balance, snow insulation, and permafrost stability, making it a key element in predicting feedbacks to the global climate system (Walker et al., 2005; Schuur et al., 2022). Recent advances illustrate both the promise and limitations of current approaches. For instance, the Boreal–Arctic Wetland Lake Database (BAWLD) distinguishes five wetland types with ecological and hydrological relevance, but is offered at a coarse 1° resolution (Olefeldt et al., 2021). High-resolution efforts such as the CircumArctic Land Cover Units map (CALU, Bartsch et al., 2024) provide 10 m classification across 23 tundra land cover types north of treeline, but is limited across the boreal biome. Collectively, these products highlight major progress in mapping Arctic vegetation (Bartsch et al., 2016, 2024; Liu et al., 2023; M. K. Raynolds et al., 2019; Walker et al., 2005), yet also underscore persistent gaps.

Despite substantial progress in land cover mapping, key gaps remain in the Arctic–Boreal Zone. Global datasets provide broad spatial coverage but rely on generalized classes that overlook important ecological differences, while regional products capture fine-scale heterogeneity but are spatially limited. This trade-off challenges applications that require both ecological detail and circumpolar continuity. Models that depend on coarse global classifications are unable to represent the diversity of vegetation communities that regulate ecosystem processes, leading to oversimplified projections of carbon and energy fluxes, permafrost dynamics, and disturbance responses. As a result, efforts to scale site-level observations to regional or circumpolar models often lose critical ecological heterogeneity, masking important differences between shrub tundra, wetland types, and boreal forest stands that strongly influence climate feedbacks (Euskirchen et al., 2016; Melvin et al., 2015; Oehri et al., 2022). Without a harmonized, ecologically detailed, and spatially continuous circumpolar dataset, our ability to predict ecosystem vulnerability and feedbacks to the global climate system remains constrained.

To address this gap, we present a workflow that fuses existing global and regional land cover products using machine learning techniques, producing a harmonized circumpolar dataset at 1 km² resolution, encompassing the time period 2000-2023. This hybrid product combines the broad spatial continuity of global maps with the ecological relevance of detailed regional classifications, providing an improved basis for modeling applications in permafrost regions. The resulting hybrid land cover product is presented at a 1 km spatial resolution, reflecting both the typical capacity of circumpolar ecosystem models and the limitations of available regional datasets, and the practical trade-offs required to maintain feasible runtimes across such large regions. While our focus is on the ABZ,

https://doi.org/10.5194/essd-2026-29
Preprint. Discussion started: 7 April 2026

the methodology is broadly applicable to other regions. We also assess the strengths and limitations of existing products and identify opportunities to enhance representation of high-latitude terrestrial systems in future datasets.

2. Materials & Methods

2.1 Study area

Our study region encompasses the ABZ, a region characterized by diverse vegetation composition spanning the northern tundra and boreal biomes (Fig. 1, Dinerstein et al., 2017). The ABZ includes approximately 4.9 × 10^6 km² of tundra ecosystems , 11.9 × 10^6 km² of boreal ecosystems, and 2.5 × 10^6 km² of other ecosystems (e.g. ice, barren) (Neigh et al., 2013). The boreal zone transitions from tundra at its northern boundary to temperate forest, steppe, or prairie in the south. Boreal forests dominate this domain, with coniferous species including spruce, pine, larch, and fir constituting the majority (~61 %), followed by mixed wood forests (~24 %) (Neigh et al., 2013; USGCRP, 2018) and pure hardwood stands (~3 %) composed of birch, alder, and aspen (USGCRP, 2018). Wetlands are also extensive across the ABZ, 3.2 x 10^6 km²of the domain, and comprised of fens (29 %), non-permafrost bogs (28 %), permafrost bogs (27 %), marshes (5 %) and tundra wetlands (12 %) (Olefeldt *et al* 2021). Tundra ecosystems are largely treeless dominated by herbaceous plants, mosses, lichens and dwarf shrubs (USGCRP, 2018; Epstein et al., 2004). Vegetation structure ranges from low-lying moss and lichen-dominated areas in colder, drier regions to more productive graminoid and shrub tundra in milder zones.

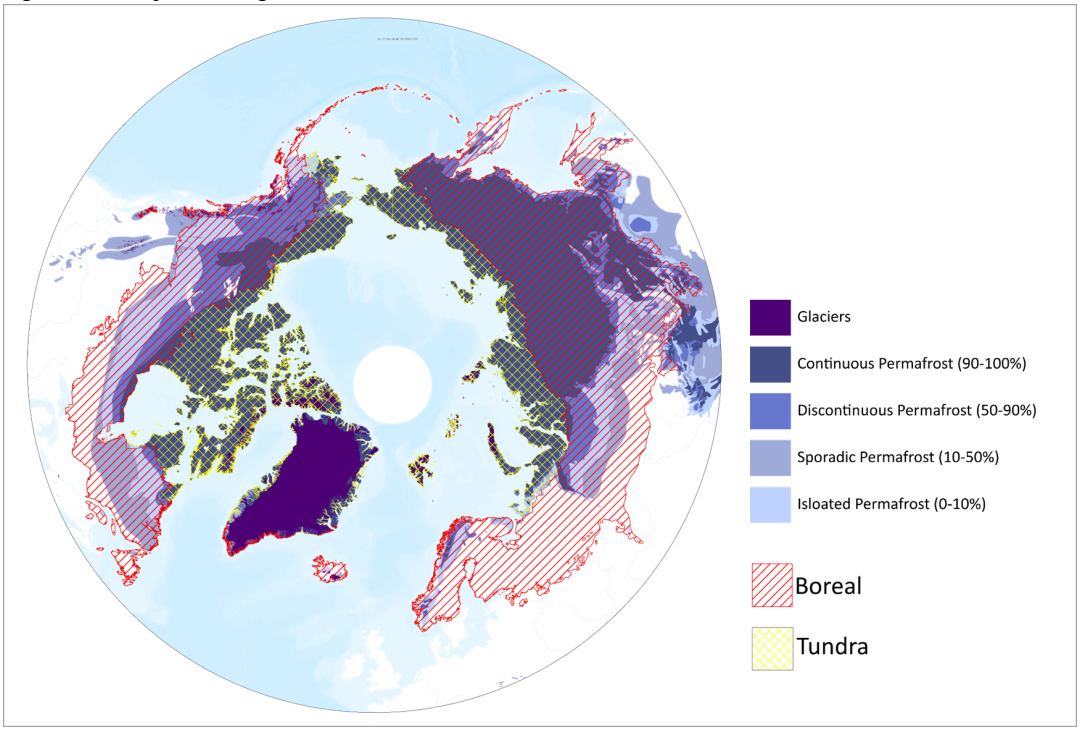

Figure 1: Study domain. The Arctic-boreal zone is defined by the boreal and tundra biomes (Dinerstein et al. 2017). Also shown is the distribution of the northern permafrost region (Brown et al., 1997) Map adapted from (USGCRP, 2018).

2.2 Methods Overview

Our goal was to develop a hybrid land cover product that combines the fine-scale land cover information from existing regional products with a global land cover layer that provides consistency across regional boundaries, in our case for the circumpolar ABZ. The workflow (Fig. 2) is comprised of five major steps: (1) pre-processing and

https://doi.org/10.5194/essd-2026-29
Preprint. Discussion started: 7 April 2026

re-projecting select land cover products to a 1 km grid using a majority rule approach, (2) reclassifying and combining global and regional products to a common legend based on agreement between global and regional products, (3) reclassifying pixels that were inconsistent between global and regional products using random forest machine learning and ancillary data variables, (4) post-classification comparison, and (5) final product compilation at 1 km resolution.

2.3 Land Cover Products and Classes

To develop the hybrid land cover product, we used a global map as the base layer to ensure a spatially continuous land cover classification. Region-specific land cover products were then selected and integrated to provide a finer-scale land cover classification scheme and to inform the reclassification process for the final product (Table 1). We chose the The European Space Agency (ESA) Climate Change Initiative Land Cover (CCI-LC) (ESA CCI-LC) as the global base map as it represents the relevant key land cover classes representative of ecosystem dynamics used in other studies related to carbon flux modeling (e.g., Virkkala et al., 2025; Virkkala et al., 2021). The global ESA CCI-LC is an annual 300 m spatial resolution land cover dataset with a time series of annual maps from 1992-2020. The map includes 22 general land cover classes defined using the Land Cover Classification System (ESA, 2016), including 7 forest types (i.e. Tree cover, needle leaved, Tree cover broadleaved) as well as shrublands, mosaic vegetation and sparse vegetation, with an overall accuracy of 71.5 % (ESA, 2017) (Table S2). To represent Arctic tundra vegetation community types, we incorporated the CALU map, which is an extension to the ESA Permafrost CCI at a 10 m resolution (ESA CCI Permafrost, Bartsch et al., 2024). The CALU map includes 23 land cover units derived from a fusion of Sentinel-1 and Sentinel-2 and separates between water bodies, wetlands, and soil moisture conditions useful for the parameterization of permafrost processes. Of the 23 vegetation classes within CALU there are 20 vegetated units including 3 wetlands classes, 2 lichen/moss, 10 classes of various shrub tundra types, 3 forest types and classes for graminoids and barren tundra. CALU is able to capture the fine-scale heterogeneity of the Arctic landscapes, which allows for a better representation of high-latitude systems and processes. We grouped the 20 vegetated land cover types in CALU into five major land cover types based on the CAVM map units: barrens, graminoid tundra, prostrate-shrub tundra, erect-shrub tundra, tall-shrub tundra, and wet-sedge tundra (M. K. Raynolds et al., 2019). CALU also has three forested land cover classifications (evergreen, deciduous, mixed), which we further classified to a specific forest type (i.e. black spruce, birch forest) depending on the classification of overlapping regional land cover products. Since CALU primarily represents the tundra biome, its applicability is limited and does not adequately capture the land cover types found within the expansive boreal region, which constitutes the majority of our study area (Table S3).

Regional products used for the boreal biome in the study were selected based on their spatial resolution, coverage, and the representativeness of land cover classes. Across North America, the main land cover products selected include the Landscape Fire and Resource Management Planning Tools (LANDFIRE) Existing Vegetation Type (EVT) map, covering all of Alaska as well as a 90 km buffer zone across the Alaska-Canada border. The LANDFIRE EVT map is derived from field observations and Landsat images at a 30 m resolution and includes over 130 land cover classes for Alaska (e.g., North American Arctic lichen tundra, Western North American boreal mesic birch-aspen forest) (LANDFIRE, 2023, Rollins, 2009) (Please see Table S4 for a full list of land cover classes). For Canada, we selected the Virtual Land Cover Engine (VLCE) product mapped annually from 1984 to 2022 across Canada's forested ecosystems, derived from Landsat surface-reflectance best-available-pixel image composites (Hermosilla et al., 2022). The VLCE map consists of 12 land cover classes at a 30-m spatial resolution, including 3 forested classes (broadleaf, coniferous, mixedwood), and 2 wetland classes (wetland, wetland-treed) (Hermosilla et al., 2018) (Table S5). To supplement the Canada VLCE, we included the lead tree species map of Canada, consisting of 37 tree species mapped across Canada at a 30-m spatial resolution, with a reported overall accuracy of 70.3 % (brus) (Table S6). The leading tree species map provides the distribution of dominant tree species per pixel derived from Landsat image composites and ancillary predictor layers such as data derived from Canada's Forest Inventory plots, and provides an overall accuracy of approximately 93 % (Hermosilla et al., 2022; Stinson et al., 2016; White et al., 2014).

We selected several regional products to cover Arctic-boreal Eurasia. For Europe, we selected the CORINE Land Cover dataset, which is a pan-European product at a 100-m spatial resolution produced from Landsat and Spot

https://doi.org/10.5194/essd-2026-29
Preprint. Discussion started: 7 April 2026

Open Access Earth System Science Data Discussions

images (CORINE, 2018) (Table S7). The CORINE product contains 44 unique land cover classes (level 3) including 3 main forest types (mixed, coniferous, and broad-leaved forest) and 5 wetland classes (inland marshes, peat bogs, salt marshes, intertidal flats, and salines) with a reported 85 % overall accuracy, with the accuracy of individual classes ranging from 95 % to 70 % (Aune-Lundberg and Strand 2021). To enhance the classification of specific forest types across Fennoscandia, we incorporated the Tree Species Map of Europe (Table S8). This map was developed by integrating plot data from the International Co-operative Programme on Assessment and Monitoring of Air Pollution Effects on Forests (ICP-Level I) and National Forest Inventory (NFI) data, resulting in a 1 km resolution product representing 20 unique species groups across Europe, with an estimated accuracy of 43–57 % (Brus et al., 2012). To supplement the classification of wetlands across Fennoscandia, we integrated the European Environmental Agency (EEA) Extended wetland ecosystem layer map, which includes 20 wetland classes across Europe at a 100 m spatial resolution for the year 2018 (EEA, 2018). For Russia, we used the land cover map of Northern Eurasia, which was created in 2000 from SPOT-4 Vegetation products and contains 26 classes at a 1km spatial resolution (Bartalev et al., 2003) (Table S9). To supplement the product with specific forest species, we incorporated the dominant tree species of Russian forests map from the Space Research Institute of the Russian Academy of Sciences which consists of 20 forest classes at a spatial resolution of 300 m (Balashov et al., 2020; Bartalev et al., 2016).

Table 1: Characteristics of the land cover products used in this study.

Dataset	Spatial Resolution	Extent	Zone	Reference Year(s)	Number of Classes	Reference
ESA CCI Land Cover 2016	300 m	Global	Global	2016	22	Lamarche et al., 2017
ESA CCI Permafrost Circumpolar Arctic Land cover Units (CALU)	10 m	Circumpolar	Arctic	2016-2023*	23	Bartsch et al. 2024
LANDFIRE	30 m	Alaska	Arctic-Boreal	2023	130	Rollins, 2009
Leading Tree Species	30 m	Canada	Boreal	2019	37	Hermosilla et al., 2022
Canada Virtual Land Cover Engine (VLCE)	30 m	Canada	Boreal	2016	23	Hermosilla et al., 2018
Canadian Wetland Inventory Map	10 m	Canada	Arctic-Boreal	2000-2016*	4	Mahdianpari et al., 2020
Tree Species Map for European Forests	1 km	Europe	Boreal	-	20	Brus et al., 2012
Corine Land Cover (CLC)	100 m	Europe	Boreal	2018	44	CORINE, 2018
European Environment Agency (EEA) Extend wetland ecosystem layer	100 m	Europe	Boreal	2018	20	EEA, 2018
Land Cover of Northern Eurasia	1 km	Russia	Arctic-Boreal	2000	26	Bartalev et al., 2003
Russia's Forests Map	300 m	Russia	Arctic-Boreal	2016	20	Bartalev et al. 2016

* Denotes land cover products that are available at an annual time scale, but a single year was selected for the project.

2.4 Pre-Processing and Initial Agreement Classification

https://doi.org/10.5194/essd-2026-29
Preprint. Discussion started: 7 April 2026

The datasets used in this study were inconsistent in their temporal and spatial resolutions as well as the land cover classifications. We addressed these differences by pre-processing the datasets to a uniform projection and spatial resolution (1 km), as well as developing a crosswalk, as discussed in the following section, of land cover classes to translate from the original classes of each regional product to that of the final product. To account for the geographical extents of each product, we approached this reclassification by region: Alaska, Canada, Iceland, Fennoscandia, Russia, and Greenland. The final list of classes and their descriptions can be found in Table 2.

Each land cover product was reprojected to WGS 1984 NSIDC EASE-Grid Global to match the projection of our input data and resampled to 1 km using a majority-rule approach. We developed a crosswalk between the regional products and the global base map to align with the general land cover classification (e.g., herbaceous). This involved grouping similar land cover classes (e.g., grasslands, croplands) within the more broad group (herbaceous). The reclassification created a harmonized classification scheme while maintaining the main representative land cover classes (forest, shrubland, herbaceous/grassland, barren, and wetland).

The first step of reclassification is based on the agreement of major land cover classifications between global and regional maps (Fig. 2). A given pixel is grouped into a new classification if both the global and regional map pixels agree at the specific land cover classification, such as evergreen needleleaf forest, broadleaf forest, shrubland, herbaceous, barren or wetland. The classification is then further refined by reassigning each pixel to a final land cover class based on its regional classification. For example, if both the global and regional maps classify the pixel as coniferous forest and a supplemental regional product identifies it as a Black Spruce Forest, then the final classification is Black Spruce Forest (the general schematic with examples can be seen in Fig. 2). However, if the global dataset classifies a pixel as evergreen needleleaf forest while the regional product identifies it as a broadleaf forest, they are in disagreement and require further processing. When such disagreements occur, we implement a random forest classification to determine the final classification of a given pixel. This further refines the classification to the final target legend of the hybrid product for a region. A detailed description of each final hybrid class, including criteria, typical vegetation, and source datasets is provided in Supplementary Table S10.

https://doi.org/10.5194/essd-2026-29
Preprint. Discussion started: 7 April 2026

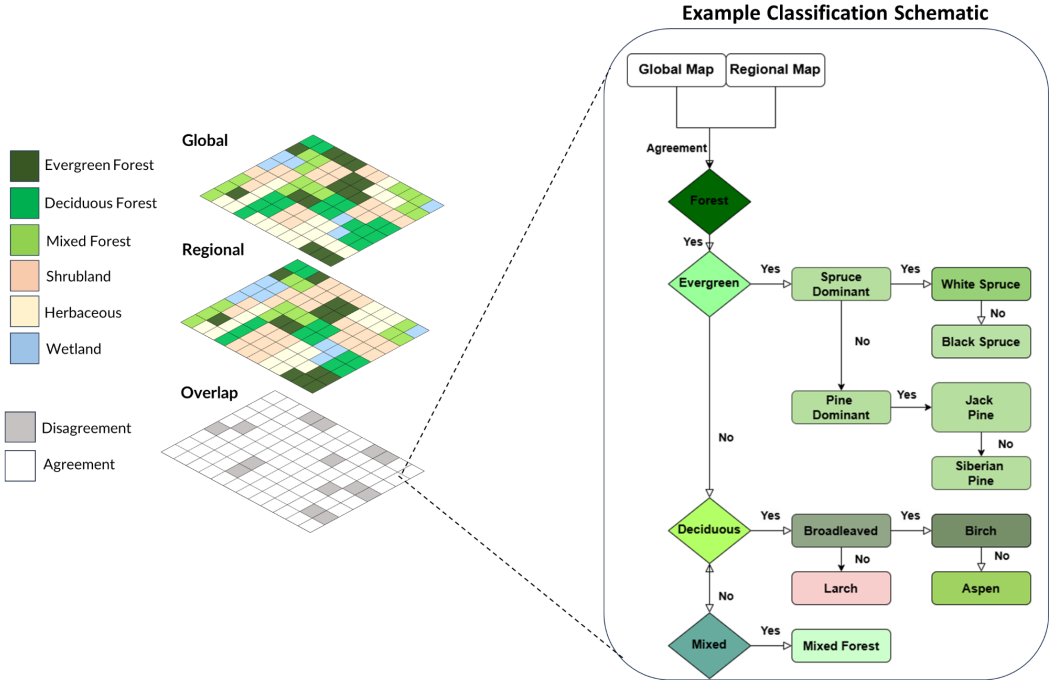

Figure 2: An overview and example of the general crosswalk between the global base map (ESA CCI-LC) and regional map(s) land cover classifications used to develop the classification scheme for the final hybrid land cover product classifications, specifically in the case when there is overlap agreement between products. This example classification schematic provides an overview for the classification of various forest type(s).

2.5 Random Forest Classification

When global and regional land cover products showed inconsistencies in classification for a given pixel, we applied a machine-learning approach to ensure consistency in vegetation classes. This was achieved by training the model with successfully classified pixels across a given region from the initial agreement step and incorporating predictor data. Random Forest is one of the most widely used supervised machine learning algorithms for land cover mapping and classification because of its ability to handle noisy and multi-source datasets (Jin et al., 2018; Maxwell et al., 2019). The random forest method is an ensemble-based classifier that uses decision trees for training and prediction. In Google Earth Engine, we used the random forest classifier. We optimized the number of trees (ntrees), selecting values between 200 and 300 based on the lowest out-of-bag (OOB) error across regions. Other hyperparameters, such as mtry (the number of variables considered at each split), were left at their default values, approximately the square root of the total number of predictor variables used in the model, which ranged from 2 to 3. We also calculated the importance score of the predictor data within the random forest classifier. The value of the importance scores are not uniform, but instead change depending on the number of sampling data and variables included within the classifier (C. Liu et al., 2020). The importance scores for each major region can be found in Fig. S1.

We included predictors within the random forest model that are strongly linked to vegetation dynamics and characteristics. Climate variables, specifically the 19 Bioclimatic variables from WorldClim, representing monthly climate data for minimum, mean, and maximum temperature, precipitation, solar radiation, wind speed, water vapor pressure, and total precipitation for 1970-2000, were included (Hijmans et al., 2005). Other variables included

https://doi.org/10.5194/essd-2026-29
Preprint. Discussion started: 7 April 2026

topography (i.e. elevation, slope, aspect) as well as descriptors of vegetation and moisture including Normalized Difference Vegetation Index (NDVI) and Normalized Difference Infrared Index (NDII) from the MOD13Q1 product of MODIS, with minimum and maximum values extracted for the period of 2000-2023 to cover the time frame of land cover products (Table S1). Training and testing data came from pixels that agreed during the initial classification agreement step between the global land cover and regional layers. We created a collection of samples that were then randomly split into groups of training (80 %) and testing (20 %) data. In total, between 500-1,200 pixels per land cover class were collected within each region. We adapted each random forest machine learning model to be region-specific to map the distribution of land cover class.

2.6 AccuracyAssessment

The accuracy of the final hybrid land cover product (including the classifications from random forest) was dependent on the quality, level of detail, and spatial extent of the regional land cover products. We first compared the proportion of agreement between the global base dataset (ESA CCI-LC) and each respective regional dataset. This comparison was conducted at a coarser land cover classification level than our final hybrid product (e.g., agreement between deciduous forest type was compared), as the ESA CCI-LC does not provide detailed information on forest species or wetland types comparable to regional products. For each region we used the confusion matrix reports to estimate accuracy metrics such as the overall accuracy (OA), which is the proportion of a given map that shows the probability that an area is classified correctly, producer accuracy (PA), which describes how well a map captures a given land cover type from the perspective of the reference data. It is the proportion of correctly classified land cover types, indicating how often a given class is missed (omission error), and user accuracy (UA), is the proportion of areas mapped as a given land cover type that truly represent that land cover type on the ground (Liu et al., 2007; Olofsson et al., 2014). These confusion matrices can be found in Fig. S2. In addition, we estimated the proportion of each land cover class of the hybrid product to compare to the global and regional products for each region, and show the accuracy metrics for the random forest classifications (Sect. 3.3).

We further assessed the accuracy of the final hybrid map to an external land cover validation product. We used the Global Land Cover Estimation (GLanCE) product, a training dataset of nearly 2 million training units spanning from 1984-2020 for seven primary and nine secondary land cover classes (Stanimirova et al. 2023). The GLanCE training dataset combines high-resolution Google Earth Imagery, time series of spectral reflectance, vegetation indices, Landsat imagery, and Landsat derived Tassled Cap transformations, which are then entries into the database representing individual pixels as a training point. Land cover classes are broken into level 1, a general classification including Water, Ice/Snow, Developed, Barren/ sparsely vegetated, Trees, Shrub, and Herbaceous; and Level 2, which provides more detail and subclasses including Water, Ice/snow, Developed, Soil, Rock, Beach/sand, Deciduous Trees, Evergreen Trees, Mixed Forest, Shrub, Grassland, Agriculture, and Moss/Lichen. For more information on the background and methods used to develop the GLanCE product refer to (Stanimirova et al. 2023).

To refine the dataset we opted for training data that did not undergo recent land cover change, had points with at least 2-3observations, and data points from 2000-2020 to better match the time frames of our collective regional and global products. We compared the GLanCE dataset to our final 1 km hybrid product, in addition to each region's main land cover product used within this study at 1 km to compare the overall accuracy of our product to other existing products.

3. Results

We present our final hybrid land cover product at a 1 km spatial resolution, developed by fusing both global and regional land cover datasets across the circumpolar region (Fig. 3). You can find an in-depth classification for each individual major region within Fig. S3.

https://doi.org/10.5194/essd-2026-29
Preprint. Discussion started: 7 April 2026

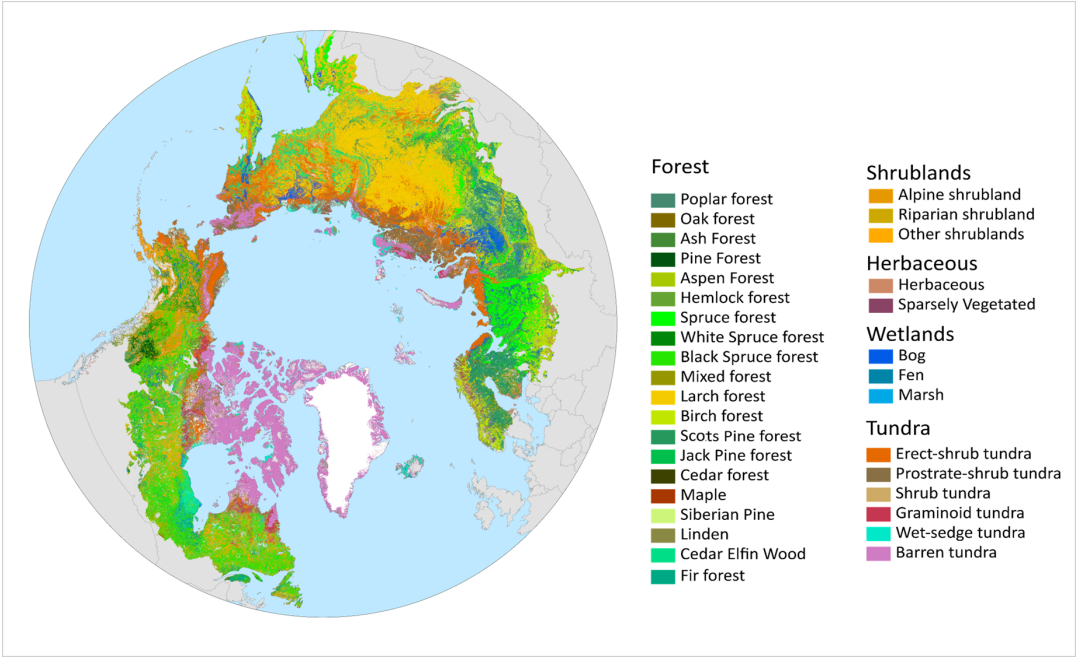

Figure 3: Final Hybrid product at 1 km resolution across the Arctic-Boreal Zone, with the integrated Circumpolar Arctic Land cover Units Map (CALU) map covering the pan-Arctic.

3.1 Overlap and agreement

When assessing the overlap between the global and regional products across the ABZ, our results show a majority agreement for each region (Fig. 4). In Alaska, the global and regional products show a 82.7 % agreement (17.3 % disagreement) across the land cover products (Fig. 4a), while in Canada there is a 79.9 % agreement (20.1 % disagreement) (Fig. 4b). There is a 79.5 % agreement (20.5 % disagreement) between global and regional products for Fennoscandia (Fig. 4c), while Russia has a 90.8 % agreement (9.2 % disagreement) amongst the land cover products, showing a large majority agreement across the region (Fig. 4d).

https://doi.org/10.5194/essd-2026-29
Preprint. Discussion started: 7 April 2026

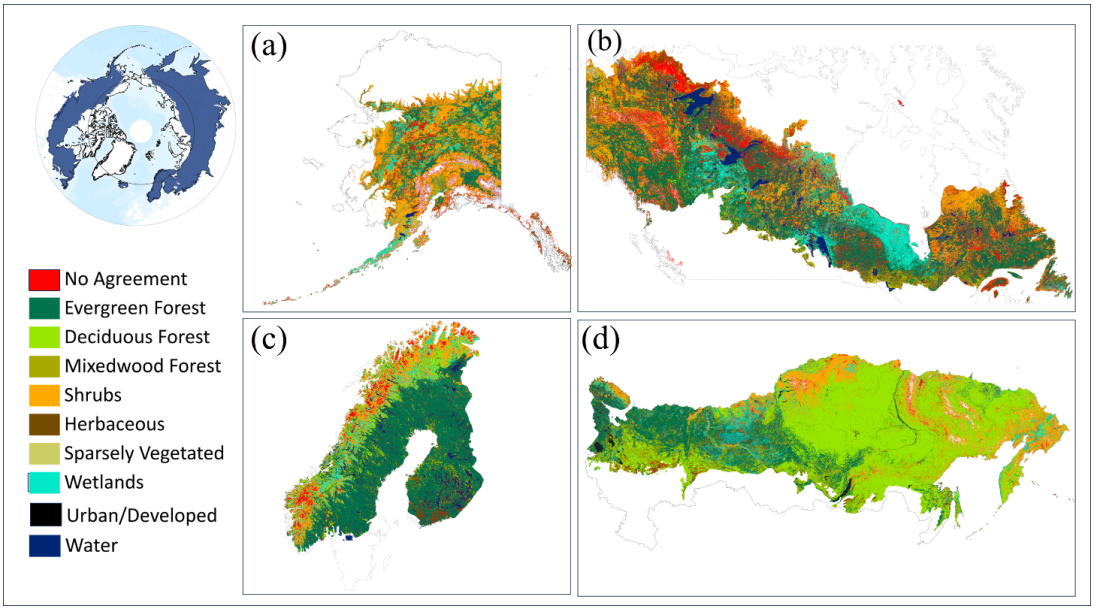

Figure 4: Agreement between the global ESA CCI-LC map and region-specific land cover products including: LANDFIRE EVT, VLCE, CORINE, Bartalev et al. 2003) across the circumpolar region at a 1 km spatial resolution. Major regions include Alaska (a), Canada (b), Fennoscandia (c), and Russia (d).

3.2 Accuracy of the hybrid map against the regional maps

The classification developed using the random forest machine learning was evaluated by comparing model outputs (i.e. the hybrid map) with the regional maps. This comparison was thus restricted to the pixels where regional and global classifications were in disagreement and the model was run. The producer's and user's accuracy metrics were derived from the confusion matrix (Fig. 5).

https://doi.org/10.5194/essd-2026-29
Preprint. Discussion started: 7 April 2026

Open Access Earth System Science Data Discussions

50-70% 71-80% 81-94% ≥95%

		Alaska		Canada		Fennoscandia		Russia		Iceland	
		UA	PA	UA	PA	UA	PA	UA	PA	UA	PA
	Land Cover Class	-									
Deciduous Forest	Poplar forest	98.00%	100.00%	98.00%	100.00%	-	-	-	-	-	-
	Ash Forest	-	-	-	-	82.00%	88.00%	-	-	-	-
	Aspen Forest	99.00%	100.00%	94.00%	96.00%	-	-	92.00%	98.00%	-	-
	Larch forest			99.00%	100.00%			89.00%	97.00%	-	-
	Birch forest	94.00%	91.00%	95.00%	99.00%	87.00%	85.00%	84.00%	92.00%	-	-
	Maple	-	-	91.00%	98.00%	-	-	100.00%	99.00%	-	-
	Linden	-	-	-	-	-	-	100.00%	100.00%	-	-
Evergreen Forest	Fir forest	-	-	98.00%	-	-	-	95.00%	94.00%	-	-
	Oak forest	-	-	-	-	-	-	100.00%	100.00%	-	-
	Pine Forest	-	-	97.00%	100.00%	87.00%	93.00%	-	-	-	-
	Hemlock forest	99.00%	100.00%	100.00%	100.00%	-	-	-	-	-	-
	Spruce forest	-	-	-	-	-	-	89.00%	65.00%	-	-
	White Spruce forest	97.00%	97.00%	98.00%	98.00%	-	-	-	-	-	-
	Black Spruce forest	95.00%	97.00%	100.00%	99.00%	-	-	-	-	-	-
	Scotts Pine forest	-	-	-	-	88.00%	83.00%	71.00%	89.00%	-	-
	Jack Pine forest	-	-	99.00%	100.00%	-	-	-	-	-	-
	Cedar forest	-	-	-	-	-	-	-	-	-	-
	Siberian Pine	-	-	-	-	-	-	91.00%	77.00%	-	-
	Cedar Elfin Wood	-	-	-	-	-	-	95.00%	100.00%	-	-
Mixed forest	Mixed forest	100.00%	98.00%	94.00%	84.00%	90.00%	90.00%	82.00%	77.00%	-	-
Shrublands	Alpine shrubland	99.00%	100.00%	94.00%	98.00%	-	-	-	-	-	-
	Riparian shrubland	100.00%	99.00%	91.00%	95.00%	-	-	97.00%	89.00%	-	-
	Other shrublands	93.00%	81.00%	97.00%	88.00%	86.00%	81.00%	86.00%	85.00%	-	-
	Erect-shrub tundra	77.00%	89.00%	91.00%	88.00%	88.00%	85.00%	87.00%	76.00%	94.00%	99.00%
	Prostrate-shrub tundra	96.00%	100.00%	-	-	90.00%	84.00%	89.00%	92.00%	100.00%	100.00%
	Shrub tundra	-	-	91.00%	92.00%	-	-	-	-	100.00%	100.00%
Herbaceous	Herbaceous	94.00%	99.00%	100.00%	100.00%	82.00%	93.00%	94.00%	92.00%	92.00%	85.00%
	Graminoid tundra	94.00%	96.00%	87.00%	91.00%	89.00%	86.00%	79.00%	88.00%	-	-
Sparse Vegetation	Sparsely Vegetated	100.00%	100.00%	97.00%	83.00%	89.00%	94.00%	-	-	-	-
	Barren tundra	89.00%	89.00%	96.00%	81.00%	100.00%	66.00%	88.00%	76.00%	100.00%	100.00%
Wetlands	Bog	88.00%	86.00%	99.00%	100.00%	85.00%	83.00%	85.00%	89.00%	77.00%	86.00%
	Fen	91.00%	89.00%	100.00%	100.00%	98.00%	87.00%	89.00%	95.00%	95.00%	50.00%
	Marsh	100.00%	99.00%	100.00%	98.00%	100.00%	69.00%	94.00%	100.00%	83.00%	85.00%
	Wet-sedge tundra	92.00%	90.00%	95.00%	95.00%	91.00%	92.00%	91.00%	89.00%	100.00%	100.00%
Developed	Developed	100.00%	88.00%	-	-	-	-	99.00%	100.00%		

Figure 5: Confusion Matrix for the Random Forest Model used to classify the remaining unclassified pixels from the initial agreement classification step for all major regions (i.e. pixels where global and regional maps didn't agree), displaying the User's Accuracy (UA), and Producer's Accuracy (PA).

Predominantly forested land cover classes were mapped with very high accuracies (>82 %). The class accuracies of herbaceous vegetation, wetlands, and tundra classes within the ABZ transition zone were classified with moderate accuracy (>50 %). Specifically, herbaceous vegetation and shrubs had high confusion errors with forest and herbaceous vegetation classes. This is expected considering the spectral similarity of these classes. Some land cover classes generated more confusion within the classifier, such as Barren tundra across most regions except Iceland, with the lowest PA at 66 % in Fennoscandia and 76 % in Russia. Within these regions the classification of Barren tundra often had higher confusion errors with other tundra classes (i.e. Graminoid tundra). Detailed confusion matrices for each region are shown in Fig. S2.

3.3 Assessment and Benchmarking of the Hybrid Land Cover Map

When comparing the proportion of major land cover classes (Fig. 6c, d) of the final hybrid product at a 1 km resolution across the boreal domain, Alaska shows a forest composition of 35% in comparison to 37% and 44 % for the regional LANDFIRE (Fig. S4b) and global ESA CCI-LC maps (Fig. S5d) , respectively. Total forest composition in the boreal region of Canada was 50% in our final product compared to 49% and 63% for the regional VLCE (Fig. S4b) and ESA CCI-LC (Fig. S5d) maps, respectively. Boreal Alaska shrublands represented 41 % of the total vegetation cover compared to 44 % and 24 % represented in LANDFIRE (Fig. S4b) and ESA CCI-LC (Fig.

https://doi.org/10.5194/essd-2026-29
Preprint. Discussion started: 7 April 2026

Open Access Earth System Science Data Discussions

S5d), respectively. Total shrublands were less prominent across boreal Canada with values of 24 % in the hybrid product compared to 22 % and 7 % from the VLCE (Fig. S4b) and ESA CCI-LC (Fig. S5d) maps, respectively.

Figure 6: Assessment of major land cover class types for our hybrid land cover product grouped by biome, Arctic (a,b) and Boreal (c,d). Panels show the total proportion of each class over the entire extent (a,c), and further subdivided by major region (b,d) including Alaska (AK), Canada (CAN), Iceland (ICE), Greenland (GRE), Fennoscandia (FEN), and Russia (RUS).

We compared the representation of five dominant land cover classes (forest, shrubland, herbaceous, sparsely vegetated, and wetlands) of the hybrid land cover product land cover types to the global and regional land cover products in their original spatial resolution. Figure 7 shows the comparison of land cover products and their

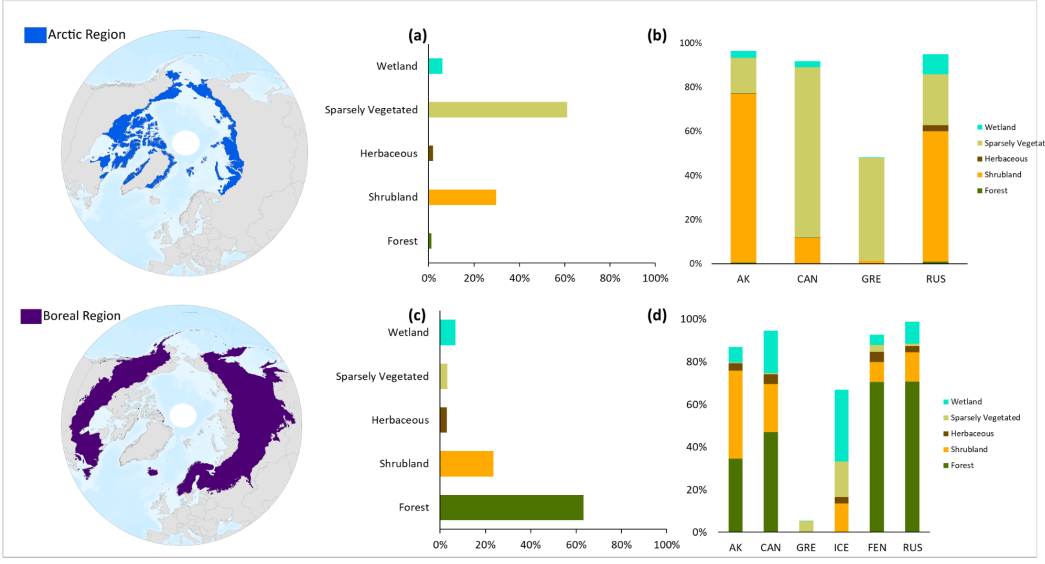

classification at four established research sites, which are sites with existing eddy covariance towers, and long-term time series of information on vegetation and soil carbon and nitrogen dynamics, including a (a) shrub tussock tundra at Eight Mile Lake in Alaska (63.8784° N, -149.2536°W), (b), black spruce peat plateau at Scotty Creek in Canada (61.3079°, 121.299° W), (c) Larch forest at Yakutsk Spasskaya in Russia (62.55° N, 129.241°E) and (d) shrub tundra at Seida in Russia (67.05° N, 62.94°E).

https://doi.org/10.5194/essd-2026-29
Preprint. Discussion started: 7 April 2026

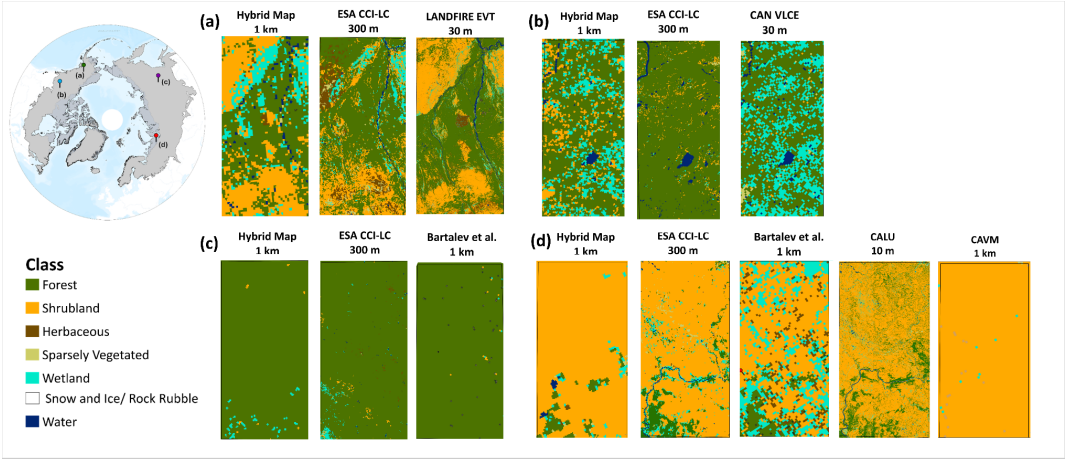

Figure 7: Comparison of the final hybrid land cover product to the regional and global products used within the study. The sites selected includes (a) shrub tundra at Eight Mile Lake in Alaska, (b) Black Spruce peat plateau at Scotty Creek in Canada, (c) Larch forest at Yakutsk Spasskaya in Russia, and (d) a shrub tundra at Seida in Russia.

Benchmarking of the hybrid map against ground truth observations

To further assess the accuracy of the final 1 km hybrid land cover map, we compared its classification against the independent GLanCE dataset. The verification included 36,986 GLanCE points located north of 40° N with valid observations between 2000 and 2020, ensuring both spatial and temporal comparability with the hybrid product. Points were further filtered to require at least 2–3 valid GLanCE observations per 1 km pixel. Figure 8a presents the confusion matrix for the Level 1 land cover classes, which shows a moderate overall accuracy (OA) of 67 % and a kappa coefficient of 0.3. In contrast, agreement decreases for the more detailed Level 2 classifications (Figure 8b), with an OA of 37 % and a kappa coefficient of 0.2, reflecting the increased difficulty of discriminating finer thematic classes. Among the Level 1 classes, tree cover exhibited the highest agreement between the hybrid map and GLanCE, accounting for 24,213 matching pixels. Most classification disagreements occur between structurally similar classes, with frequent confusion between sparsely vegetated and herbaceous categories, highlighting known challenges in separating these land cover types using satellite-based classifications.

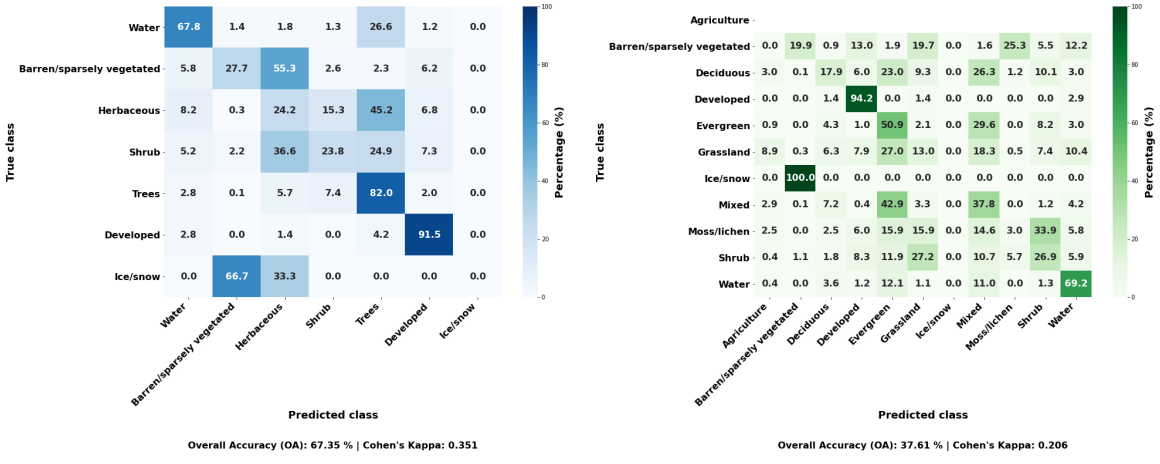

https://doi.org/10.5194/essd-2026-29
Preprint. Discussion started: 7 April 2026

Figure 8 : Confusion matrices for the 1 km hybrid land cover map (Observed class) verified against the Global Land Cover Estimation (GLanCE) dataset (Predicted class) for (a) level 1 land cover classifications and (b) level 2 land cover classes. Rows with only zeros present appear white.

Similar patterns are observed for the regional products showing an overall decline in OA when comparing between level 1 and level 2 land cover classifications. When comparing the accuracy of the GLanCE dataset to the regional land cover products used within the study, we see an overall accuracy of 39% for the Alaskan LANDFIRE product (Fig. S6a), 29.6% for the Canadian Hermosilla et al. 2018 product (Fig. S6c), 77.8% for the CORINE land cover product (Fig. S6e), and 69.5% for the Bartalev et al. product (Fig. S6g), highlighting the range of OA and kappa coefficients are relatively similar when comparing them directly to the regional products.

4. Discussion

The development of our hybrid land cover product at a 1 km spatial resolution provides a valuable synthesis of both global and regional land cover datasets across the ABZ. The results indicate a high degree of agreement between global and regional products, yet notable differences emerge both regionally and across specific land cover classes.

4.1 Integration Approach for a Hybrid Land Cover Product

We present an integration approach to generate a hybrid land cover product at 1 km spatial resolution, specifically tailored to vegetation classifications for regional model applications and other research investigations. Our main objective was to introduce an adaptable approach that enables the combination of multiple land cover datasets with varying spatial resolutions, thematic content, and sources, resulting in a unified hybrid classification system. Our final product exhibited reasonable accuracy across regions when compared to both the global and corresponding regional maps.

The general harmonization approach of our workflow is reproducible and can be applied to other study regions at both regional and global scales. To accurately represent the diverse vegetation communities of the ABZ, integrating multiple local and regional land cover maps is essential. Compared to the Arctic region, where substantial efforts have been made to represent tundra vegetation in detail and at high spatial resolutions (Bartsch et al., 2024; A. Liu et al., 2023; Raynolds & Walker, 2008), boreal vegetation has remained challenging to classify consistently mainly because of a lack of detailed, fine-resolution classification across international borders. As new or updated regional and global products become available, our approach has the flexibility to incorporate these data, leading to continuous refinement and enhancement of the final product and providing more refined and updated land cover classifications.

4.2 Regional Disparities in Agreement and Model Performance

Agreement between global and regional products used to develop our model varies by region, with Russia exhibiting the highest rates (9.5 %), compared to Alaska, Canada and Fennoscadia (17.3%, 20.1% and 20.5% respectively). These regional differences in accuracy can be attributed to differences in the spatial resolution and time-stamp between global and regional products. Land cover heterogeneity documented by fine-scale products could result in a majority land cover class different from a classification developed at coarser scale (Li et al. 2023), especially across landscapes characterized by high spatial variability, such as polygonal tundra in the arctic (Lara et al., 2020), or wetland complexes in the boreal biomes (Jorgenson et al., 2018). Differences in epoques covered by the various land cover products used in this study could also largely contribute to the differences in land cover classes as disturbances such as wildfire or abrupt permafrost thaw, and land use change (e.g. oil exploration or forest

https://doi.org/10.5194/essd-2026-29
Preprint. Discussion started: 7 April 2026

management activities) can trigger abrupt land cover change and transitions resulting from successional trajectory (e.g., Johnstone et al., 2010; Johnstone et al., 2016).

Across the Alaskan Boreal extent, in areas where there was higher disagreement between global (ESA CCI-LC) and regional products (LANDFIRE), the greatest source of disagreement came from misclassification between coniferous forest and mixed forest, at 13 % of pixel disagreement. Similarly, across the Canadian Boreal extent, the areas of highest disagreement were those between shrublands (VLCE) and coniferous forest (ESA CCI-LC) at 8 %, and disagreement between coniferous forest and mixed forest classifications at 6 %. This disagreement among similar land cover classes has often been attributed to confusion from similar spectral signatures in the satellite imagery. This is especially true for differences between mixed and coniferous forest, as well as deciduous forest, shrublands, shrub-covered wetlands, and herbaceous classes (Latifovic et al., 2017; Wang et al., 2019), but may also reflect differences in the acquisition years of the underlying land cover products, which can mix successional stages and pre-disturbance states.

Comparisons of land cover class representation show that boreal forest coverage in Alaska is broadly consistent across datasets, with the hybrid and LANDFIRE products both estimating forest extent at 44 %, and the global ESA product estimating a slightly higher value of 48 %. In contrast, shrubland coverage differs substantially among datasets, with the hybrid product indicating a much larger shrubland extent (44 %) compared to the ESA product (24 %), suggesting the importance of integrating regional datasets to more accurately reflect dominant vegetation classifications. These differences in classification can be observed across the ABZ as shown in Fig. S4, specifically showcasing the general underestimation of wetlands within the ESA CCI-LC product. These differences have significant implications for ecological modeling, as over- or underestimation of land cover classes directly affects simulations of ecosystem processes, such as carbon fluxes and vegetation dynamics (Jung et al., 2006; Pérez-Hoyos et al., 2012). Wetlands, in particular, remain one of the most challenging land cover types to classify accurately due to their fine-scale heterogeneity, seasonal variability, and often ambiguous spectral signatures (Mahdavi et al., 2018). Our hybrid product takes advantage of regional classification schemes and ancillary data layers to improve the delineation of wetland classes. For example, in North America across the boreal extent, our hybrid map estimates wetlands at 21 %, which is closely aligned with the 22 % wetland extent reported in BAWLD, while our hybrid map shows 21 % and BAWLD 28 % across Eurasia boreal extent (Olefeldt et al., 2021). This consistency suggests that our approach can effectively capture the spatial distribution of wetlands, enhancing the reliability of wetland representation for process-based models and climate assessments. While this suggests a coherent representation of wetland distribution at broad scales, some variation is expected given that several regional land cover datasets do not explicitly include wetland classes, constraining direct spatial comparison for this category. Nevertheless, the hybrid approach integrates ancillary wetness and vegetation indices to enhance wetland delineation where regional information is lacking. A more refined understanding of wetland extent and distribution is particularly critical for permafrost modeling and methane emission projections, where wetland dynamics play a disproportionate role in influencing carbon-climate feedbacks.

Certain regions exhibit higher levels of disagreement, particularly in transitional zones where land cover classes are more challenging to delineate (Heiskanen, 2008; Herold et al., 2008; Prestele et al., 2016). For example, shrub tundra and herbaceous wetlands demonstrate higher classification errors due to spectral similarities with adjacent vegetation classes (Latifovic et al., 2017). The confusion matrix highlights (Fig. 5) how barren tundra, particularly in Fennoscandia and Russia, is frequently misclassified as graminoid tundra by the random forest model. This misclassification underscores the limitations of optical remote sensing in distinguishing subtle land cover transitions.

The application of the random forest classifier was crucial for resolving unclassified pixels, especially in regions with sparse or inconsistent data coverage. Notably, locations such as black spruce peat plateaus in Canada required machine learning-based estimations due to their unique spectral and structural characteristics. While the classifier performed well for forested classes (>82 % accuracy), moderate accuracies (>50 %) were observed for herbaceous wetlands and tundra, reflecting inherent classification challenges in these environments.

Beyond classification challenges, differences in spatial resolution amongst input datasets also contribute to regional inconsistencies. Global products such as the ESA-CCI-LC are at a coarser resolution that inherently

https://doi.org/10.5194/essd-2026-29
Preprint. Discussion started: 7 April 2026

neglects fine-scale heterogeneity in tundra, wetland, and herbaceous shrub mosaic landscapes. Such landscapes exhibit high variability in vegetation and hydrological composition, features that are critical for further understanding carbon and permafrost processes. By integrating fine-scale datasets, our hybrid land cover product captures the broad-scale spatial patterns across the ABZ at a 1 km resolution. Nonetheless, fine-scale heterogeneity such as microtopography and wetness gradients continues to influence permafrost carbon dynamics and energy fluxes (Treat et al., 2018; Muster et al., 2019; Nitzbon et al., 2020). Continued use of high-resolution datasets will further enhance the product's ability to represent patterned and transitional landscapes, improving the ecological realism of regional carbon and energy modeling.

4.3 External Validation with the GLanCE Dataset

To further evaluate the accuracy and generalizability of the hybrid land cover product, we compared it against the independent Global Land Cover Estimation (GLanCE) dataset (Stanimirova et al., 2023). GLanCE provides an extensive global training dataset based on multi-decadal Landsat observations and high-resolution reference imagery, offering an effective benchmark for assessing classification consistency across broad regions. When comparing GLanCE with the regional products used in this study, the OA ranged from 29–78%, with the highest values found for the CORINE and Bartalev et al. maps and lower accuracies for the North American products (LANDFIRE, VLCE). The hybrid product's OA falls within the upper range of these validation results, suggesting that the integration of regional and global datasets improves representation consistency across circumpolar regions without introducing significant new classification errors.

The comparison with GLanCE also highlights remaining challenges for high-latitude land cover mapping. Although our hybrid approach enhances consistency across data sources, the moderate external accuracy underscores the importance of incorporating additional training data and higher-resolution ancillary information (e.g., LiDAR, SAR) in future refinements. Nevertheless, the validation results support the robustness of the hybrid dataset for large-scale applications, such as ecosystem modeling and carbon budget assessments, where regional agreement and relative class distribution are more critical than exact pixel-level correspondence.

Relevance for Carbon Modeling and Ecosystem Dynamics

From a carbon modeling perspective, land cover maps that contain a detailed and accurate classification of various vegetation community types are important due to their unique contributions to carbon and methane dynamics. Forested and shrubland regions play a crucial role in CO_2 sequestration due to their high biomass density and substantial carbon storage in both aboveground and belowground pools. Forests act as significant carbon sinks, with global estimates indicating that they sequester approximately 7.8 ± 0.4 Pg C annually (Pan et al., 2024). Boreal and temperate forests, in particular, store vast amounts of carbon in biomass and soils. In high-latitude regions, boreal forests and shrublands are closely linked to large soil and permafrost carbon stocks (Hugelius et al., 2020), making accurate representation of these vegetation types especially important for models seeking to simulate carbon dynamics under ongoing climate change. Shrub expansion in high-latitude tundra regions due to climate change has been linked to increased CO_2 uptake during the growing season (Myers-Smith et al., 2011), however, these ecosystems can also act as sources of methane under conditions of water saturation, particularly in permafrost regions (Treat et al., 2018). In contrast, wetlands and peatlands, which store about one-third of the world's soil carbon (Yu, 2012), are also significant sources of methane emissions, especially under warmer and wetter conditions (Turetsky et al., 2014).

Improving the spatial resolution of wetland land cover mapping can significantly enhance model accuracy by reducing the amount of heterogeneity not captured within pixels, leading to more accurate ecosystem representation (e.g., Kuhn et al., 2021). Land cover products, such as BAWLD and the Circumpolar Arctic Land Cover Unit (CALU) dataset, provide refined classifications of wetland, lake, and river ecosystems (Bartsch et al.,

https://doi.org/10.5194/essd-2026-29
Preprint. Discussion started: 7 April 2026

2024; Olefeldt et al., 2021). These datasets incorporate expert knowledge and spatial data to differentiate landscape classes based on distinct hydrological and biogeochemical characteristics, enabling improved modeling of current and future methane emissions. However, global models disagree as to the magnitude and spatial distribution of emissions, due to uncertainties in wetland area and emissions per unit area (Bohn et al 2015).

Accurate representation of these dynamics in carbon cycle models is crucial for improving projections of future climate, and understanding these distributions accurately is fundamental for process-based models that simulate greenhouse gas fluxes in Arctic and Boreal ecosystems. The hybrid land cover product, with its improved representation of fine-scale vegetation classes, enhances the capacity of these models to capture spatial variability in these complex systems. Despite its advantages, uncertainties remain with this approach. Differences in time periods and methodologies across the global and regional datasets introduce inconsistencies in land cover classification. Additionally, classification errors due to spectral similarities between vegetation classes highlight the need for continued refinement, potentially through the integration of ancillary datasets such as LiDAR or SAR imagery.

Uncertainties

While integrating multiple land cover datasets may enhance spatial representation, it introduces challenges related to classification consistency/harmonization, scale and accurate representation of changes in vegetation dynamics. In particular, the fusion of global and regional land cover products can result in boundary mismatches where regional products meet, as illustrated by the transition along the Alaska–Canada border visible in our hybrid map. This example highlights both the benefit of incorporating higher-resolution regional information and a key limitation, namely that inconsistencies in classification schemes and mapping approaches among regional products can propagate into the fused product. Studies have shown that the classification accuracy of global land cover products varies across different regions. For example the ESA CCI-LC product shows an overall accuracy of 63.5 % in the Arctic region, highlighting the need for careful consideration when integrating more detailed regional products to supplement the classification of these regions (Liang et al 2019).

Our hybrid land cover product's 1 km resolution balances spatial detail with computational efficiency, but may not capture fine scale heterogeneity in certain landscapes. Less represented land cover types, such as fens or patchy wetlands may be underrepresented when aggregated to coarser resolutions. Resampling from finer resolutions (i.e. 10 m to 10 km) can significantly alter the proportion of these heterogeneous classes. For instance, the proportion of wetland cover in the CALU dataset decreases from approximately 9 % at 10 m resolution to 6.3 % at 1km and further to 5.5 % at 10 km. These changes should be considered when integrating datasets at varying resolutions or when applying the datasets to broad regions.

Given these uncertainties, users applying this dataset for carbon flux modeling, biodiversity assessments, or land cover change analyses should account for potential biases introduced by classification errors, resolution limitations, and temporal inconsistencies. While this hybrid dataset improves Arctic and boreal land cover representation compared to global datasets alone, ongoing refinements are needed to enhance the accuracy of underrepresented classes and transitional zones. Understanding these dataset uncertainties is essential for informed application in ecological and climate research. By acknowledging and addressing these limitations, users can better interpret the data and contribute to ongoing efforts to refine land cover mapping in Arctic and boreal regions.

Conclusion

Accurate land cover maps are essential for understanding ecosystem structure, dynamics, and change, yet comprehensive, high-resolution maps remain scarce across many of Earth's biomes, including the ABZ. To address this gap, we present a new hybrid land cover dataset spanning the entire ABZ at a moderate spatial resolution of 1 km. This circumpolar product integrates and harmonizes multiple existing global and regional land cover datasets, improving representation of key vegetation types, including shrub tundra and boreal forest communities, which are often underrepresented or misclassified in coarser-resolution products. Our dataset distinguishes 35 land cover classes tailored to ecological and modeling applications, offering improved accuracy and spatial consistency across geopolitical boundaries.

https://doi.org/10.5194/essd-2026-29
Preprint. Discussion started: 7 April 2026

The underlying methodology combines a multi-step integration process with machine learning-based refinement, leveraging agreement between validated products to enhance reliability. While this workflow supports the dataset's development, our primary contribution is the hybrid product itself—designed to support ecosystem modeling, permafrost and carbon assessments, and land-atmosphere interaction studies. This dataset serves as a valuable resource for the scientific community working in the ABZ, and future updates may incorporate additional observational inputs to further improve resolution and thematic detail.

Author contributions

VB conceptualized the paper with the support of EJ, HG, BR. Co-authors EJ, HG, BR, BM, JW, SN, AB, AMV, JR reviewed and provided feedback and content to the manuscript.

Competing Interests

The authors declare that they have no conflict of interest.

Acknowledgements

This work was funded by the Quadrature Climate Foundation (grant no. 01-21-000094) and funding catalyzed by the TED Audacious Project (Permafrost Pathways), with additional support from Google.org's Impact Challenge for Climate Innovation Program, and the Bonanza Creek Long Term Ecological Research Program (grant no. DEB-2224776).

Data Availability

The dataset: A hybrid circumpolar 1 km land cover product has been made available to the Zenodo platform and can be accessed via https://doi.org/10.5281/zenodo.17968808 (Briones et al., 2025). The data is available in GeoTIFF format at a 1 km spatial resolution.

Supplementary Materials

References

Aune-Lundberg, L., and Strand, G.-H.:The content and accuracy of the CORINE Land Cover dataset for Norway. International Journal of Applied Earth Observation and Geoinformation, 96, 102266. https://doi.org/10.1016/j.jag.2020.102266, 2021.

Balashov, I., Bartalev, S., Bartalev, S., Burtsev, M., Vorushilov, I., Egorov, V., Kashnitskii, A., Khovratovich, T., Khvostikov, S., Kobets, D., Loupian, E., Saigin, I., Senko, K., Stytsenko, F., Sychugov, I., and Zharko, V.: Vega-Les Information System. Actual Features and Future Evolution. IOP Conference Series: Earth and Environmental Science, 507(1), 012002. https://doi.org/10.1088/1755-1315/507/1/012002, 2020.

Balshi, M. S., Mcguire, A. D., Duffy, P., Flannigan, M., Kicklighter, D. W., & Melillo, J.:Vulnerability of carbon storage in North American boreal forests to wildfires during the 21st century. Global Change Biology, 15(6), 1491–1510. https://doi.org/10.1111/j.1365-2486.2009.01877.x, 2009.

https://doi.org/10.5194/essd-2026-29
Preprint. Discussion started: 7 April 2026

582 Bartalev, S. A., Belward, A. S., Erchov, D. V., & Isaev, A. S.: A new SPOT4-VEGETATION derived land cover
583 map of Northern Eurasia. International Journal of Remote Sensing, 24(9), 1977–1982.
584 https://doi.org/10.1080/0143116031000066297, 2003.
585 Bartalev, S. A., Plotnikov, D. E., & Loupian, E. A.: Mapping of arable land in Russia using multi-year time series of
586 MODIS data and the LAGMA classification technique. Remote Sensing Letters, 7(3), 269–278.
587 https://doi.org/10.1080/2150704X.2015.1130874, 2016.
588 Bartsch, A., Efimova, A., Widhalm, B., Muri, X., von Baeckmann, C., Bergstedt, H., Ermokhina, K., Hugelius, G.,
589 Heim, B., & Leibman, M.: Circumarctic land cover diversity considering wetness gradients. Hydrology and
590 Earth System Sciences, 28(11), 2421–2481. https://doi.org/10.5194/hess-28-2421-2024, 2024.
591 Bartsch, A., Höfler, A., Kroisleitner, C., and Trofaier, A.: Land cover mapping in northern high latitude permafrost
592 regions with satellite data: Achievements and remaining challenges. Remote Sensing, 8(12), 979.
593 https://doi.org/10.3390/rs8120979, 2016.
594 Betts, R. A.: Offset of the potential carbon sink from boreal forestation by decreases in surface albedo. Nature,
595 408(6809), Article 6809. https://doi.org/10.1038/35041545. 2000.
596 Bohn, T. J., Melton, J. R., Ito, A., Kleinen, T., Spahni, R., Stocker, B. D., Zhang, B., Zhu, X., Schroeder, R.,
597 Glagolev, M. V., et al.:WETCHIMP-WSL: Intercomparison of wetland methane emissions models over
598 West Siberia. Biogeosciences, 12(11), 3321–3349. https://doi.org/10.5194/bg-12-3321-2015, 2015
599 Bonfils, C. J. W., Phillips, T. J., Lawrence, D. M., Cameron-Smith, P., Riley, W. J., and Subin, Z. M.: On the
600 influence of shrub height and expansion on northern high latitude climate. Environmental Research Letters,
601 7(1), 015503. https://doi.org/10.1088/1748-9326/7/1/015503, 2012.
602 Briones V, Genet H, Jafarov E E, Rogers B, Watts J D, Virkkala A-M, Bartsch A, Maglio B C, Natali S M and Rady
603 J.: Hybrid Land Cover Product: A hybrid circumpolar 1 km land cover product Online:
604 https://zenodo.org/records/15231293. 2025.
605 Brown, J., Sidlauskas, F. J., and Delinski, G.: Circum-Arctic map of permafrost and ground ice conditions, map,
606 National Snow and Ice Data Center, Boulder, CO, USA, 1997.
607 Brus, D. J., Hengeveld, G. M., Walvoort, D. J. J., Goedhart, P. W., Heidema, A. H., Nabuurs, G. J., and Gunia, K.:
608 mapping of tree species over Europe. European Journal of Forest Research, 131(1), 145–157.
609 https://doi.org/10.1007/s10342-011-0513-5, 2012.

https://doi.org/10.5194/essd-2026-29
Preprint. Discussion started: 7 April 2026

610 Carman, T. B., Genet, H., Rutter, R. A., Jafarov, E., Euskirchen, E., Maglio, B., Clein, J., Briones, V., and others:
611 DVMDOSTEM: a terrestrial ecosystem model designed to represent Arctic, boreal and permafrost
612 ecosystem dynamics, in review, J. Open Source Software., available at:
613 https://joss.theoj.org/papers/de6adf41412b7028d7be0a2064ea78cf, 2025.
614 Dinerstein, E., Olson, D., Joshi, A., Vynne, C., Burgess, N. D., Wikramanayake, E., Hahn, N., et al.: An ecoregion-
615 based approach to protecting half the terrestrial realm. BioScience, 67(6), 534–545.
616 https://doi.org/10.1093/biosci/bix014, 2017.
617 Elmendorf, S. C., Henry, G. H. R., Hollister, R. D., Björk, R. G., Boulanger-Lapointe, N., Cooper, E. J.,
618 Cornelissen, J. H. C., Day, T. A., Dorrepaal, E., Elumeeva, T. G., et al.:Plot-scale evidence of tundra
619 vegetation change and links to recent summer warming. Nature Climate Change, 2(6), 453–457.
620 https://doi.org/10.1038/nclimate1465, 2012.
621 Epstein, H. E., Calef, M. P., Walker, M. D., Stuart Chapin III, F., and Starfield, A. M.: Detecting changes in Arctic
622 tundra plant communities in response to warming over decadal time scales. Global Change Biology, 10(8),
623 1325–1334. https://doi.org/10.1111/j.1529-8817.2003.00810.x, 2004.
624 ESA: Land Cover CCI Product User Guide Version 2.0, available at:
625 http://maps.elie.ucl.ac.be/CCI/viewer/download/ESACCI-LC-Ph2-PUGv2_2.0.pdf, last access: 16 April
626 2024.
627 European Environment Agency: CORINE Land Cover 2018 (raster 100 m), Europe, 6-yearly – version 2020_20u1,
628 May 2020, https://doi.org/10.2909/960998c1-1870-4e82-8051-6485205ebbac, 2020.
629 European Environment Agency (EEA): Extended wetland ecosystem layer, Prod-ID: DAT-276-en, published 30
630 June 2022, available at: https://www.eea.europa.eu/en/datahub/datahubitem-view/b9399908-557a-47a8-
631 954a-958dabeaf1b6, last access: 05 June 2024.
632 Euskirchen, E. S., Bennett, A. P., Breen, A. L., Genet, H., Lindgren, M. A., Kurkowski, T. A., McGuire, A. D., and
633 Rupp, T. S.: Consequences of changes in vegetation and snow cover for climate feedbacks in Alaska and
634 northwest Canada. Environmental Research Letters, 11(10), 105003. https://doi.org/10.1088/1748-
635 9326/11/10/105003, 2016.
636 Heimann, M., and Reichstein, M.: Terrestrial ecosystem carbon dynamics and climate feedbacks. Nature, 451(7176),
637 Article 7176. https://doi.org/10.1038/nature06591, 2008.

https://doi.org/10.5194/essd-2026-29
Preprint. Discussion started: 7 April 2026

638 Heiskanen, J.: Evaluation of global land cover data sets over the tundra–taiga transition zone in northernmost
639 Finland. International Journal of Remote Sensing, 29(13), 3727–3751.
640 https://doi.org/10.1080/01431160701871104, 2008.
641 Hermosilla, T., Wulder, M. A., White, J. C., and Coops, N. C.: Land cover classification in an era of big and open
642 data: Optimizing localized implementation and training data selection to improve mapping outcomes.
643 Remote Sensing of Environment, 268, 112780. https://doi.org/10.1016/j.rse.2021.112780, 2022.
644 Hermosilla, T., Wulder, M. A., White, J. C., Coops, N. C., and Hobart, G. W.: Disturbance-informed annual land
645 cover classification maps of Canada's forested ecosystems for a 29-Year Landsat time series. Canadian
646 Journal of Remote Sensing, 44(1), 67–87. https://doi.org/10.1080/07038992.2018.1437719, 2018.
647 Herold, M., Mayaux, P., Woodcock, C. E., Baccini, A., and Schmullius, C.: Some challenges in global land cover
648 mapping: An assessment of agreement and accuracy in existing 1 km datasets. Remote Sensing of
649 Environment, 112(5), 2538–2556. https://doi.org/10.1016/j.rse.2007.11.013, 2008.
650 Hijmans, R. J., Cameron, S. E., Parra, J. L., Jones, P. G., and Jarvis, A.: Very high resolution interpolated climate
651 surfaces for global land areas. International Journal of Climatology, 25(15), 1965–1978.
652 https://doi.org/10.1002/joc.1276, 2005.
653 Horvath, P., Tang, H., Halvorsen, R., Stordal, F., Tallaksen, L. M., Berntsen, T. K., and Bryn, A.: Improving the
654 representation of high-latitude vegetation distribution in dynamic global vegetation models.
655 Biogeosciences, 18(1), 95–112. https://doi.org/10.5194/bg-18-95-2021, 2021.
656 Hugelius, G., Loisel, J., Chadburn, S., Jackson, R. B., Jones, M., MacDonald, G., Marushchak, M., Olefeldt, D.,
657 Packalen, M., Siewert, M. B., Treat, C., Turetsky, M., Voigt, C., and Yu, Z.: Large stocks of peatland
658 carbon and nitrogen are vulnerable to permafrost thaw. Proceedings of the National Academy of Sciences,
659 117(34), 20438–20446. https://doi.org/10.1073/pnas.1916387117, 2020.
660 Intergovernmental Panel on Climate Change.: Climate change and land: IPCC special report on climate change,
661 desertification, land degradation, sustainable land management, food security, and greenhouse gas fluxes in
662 terrestrial ecosystems (1st ed.). Cambridge University Press. https://doi.org/10.1017/9781009157988, 2022.
663 Jin, Y., Liu, X., Chen, Y., and Liang, X.: Land-cover mapping using Random Forest classification and incorporating
664 NDVI time-series and texture: A case study of central Shandong. International Journal of Remote Sensing,
665 39, 1–21. https://doi.org/10.1080/01431161.2018.1490976, 2018.

https://doi.org/10.5194/essd-2026-29
Preprint. Discussion started: 7 April 2026

666 Johnstone, J. F., Allen, C. D., Franklin, J. F., Frelich, L. E., Harvey, B. J., Higuera, P. E., Mack, M. C.,
667 Meentemeyer, R. K., Metz, M. R., Perry, G. L., Schoennagel, T., and Turner, M. G.: Changing disturbance
668 regimes, ecological memory, and forest resilience. Frontiers in Ecology and the Environment, 14(7), 369–
669 378. https://doi.org/10.1002/fee.1311, 2016.
670 Johnstone, J. F., Hollingsworth, T. N., Chapin Iii, F. S., & Mack, M. C. Changes in fire regime break the legacy lock
671 on successional trajectories in Alaskan boreal forest. Global Change Biology, 16(4), 1281–1295.
672 https://doi.org/10.1111/j.1365-2486.2009.02051.x, 2010.
673 Joshi, N., Baumann, M., Ehammer, A., Fensholt, R., Grogan, K., Hostert, P., Jepsen, M., Kuemmerle, T., Meyfroidt,
674 P., Mitchard, E., Reiche, J., Ryan, C., and Waske, B.: A review of the application of optical and radar
675 remote sensing data fusion to land use mapping and monitoring, Remote Sens., 8, 70,
676 https://doi.org/10.3390/rs8010070, 2016.
677 Jorgenson, J. C., Jorgenson, M. T., Boldenow, M. L., & Orndahl, K. M. Landscape Change Detected over a Half
678 Century in the Arctic National Wildlife Refuge Using High-Resolution Aerial Imagery. Remote Sensing,
679 10(8), 1305. https://doi.org/10.3390/rs10081305, 2018.
680 Jung, M., Henkel, K., Herold, M., and Churkina, G.: Exploiting synergies of global land cover products for carbon
681 cycle modeling. Remote Sensing of Environment, 101(4), 534–553.
682 https://doi.org/10.1016/j.rse.2006.01.020, 2006.
683 Kåresdotter, E., Destouni, G., Ghajarnia, N., Hugelius, G., and Kalantari, Z.: Mapping the vulnerability of Arctic
684 wetlands to global warming. Earth's Future, 9(5), e2020EF001858. https://doi.org/10.1029/2020EF001858,
685 2021.
686 Kuhn, M. A., Varner, R. K., Bastviken, D., Crill, P., MacIntyre, S., Turetsky, M., Walter Anthony, K., McGuire, A.
687 D., and Olefeldt, D.: BAWLD-CH_4: A comprehensive dataset of methane fluxes from boreal and Arctic
688 ecosystems. Earth System Science Data, 13(11), 5151–5189. https://doi.org/10.5194/essd-13-5151-2021,
689 2021.
690 Lamarche, C., Santoro, M., Bontemps, S., D'Andrimont, R., Radoux, J., Giustarini, L., Brockmann, C., Wevers, J.,
691 Defourny, P., and Arino, O.: Compilation and validation of SAR and optical data products for a complete
692 and global map of inland/ocean water tailored to the climate modeling community. Remote Sensing, 9(1),
693 Article 1. https://doi.org/10.3390/rs9010036, 2017.

https://doi.org/10.5194/essd-2026-29
Preprint. Discussion started: 7 April 2026

694 Lara, M. J., McGuire, A. D., Euskirchen, E. S., Genet, H., Yi, S., Rutter, R., Iversen, C., Sloan, V., & Wullschleger,
695 S. D. Local-scale Arctic tundra heterogeneity affects regional-scale carbon dynamics. Nature
696 Communications, 11(1), 4925. https://doi.org/10.1038/s41467-020-18768-z, 2020.
697 Latifovic, R., Pouliot, D., and Olthof, I.: Circa 2010 land cover of Canada: Local optimization methodology and
698 product development. Remote Sensing, 9(11), Article 11. https://doi.org/10.3390/rs9111098, 2017.
699 Li, R., Gao, X., Shi, F., & Zhang, H. Scale Effect of Land Cover Classification from Multi-Resolution Satellite
700 Remote Sensing Data. Sensors, 23(13), 6136. https://doi.org/10.3390/s23136136, 2023.
701 Liang, L., Liu, Q., Liu, G., Li, H., and Huang, C.: Accuracy evaluation and consistency analysis of four global land
702 cover products in the Arctic region. Remote Sensing, 11(12), Article 12.
703 https://doi.org/10.3390/rs11121396, 2019.
704 Liu, A., Moore, J. C., and Chen, Y.: PInc-PanTher estimates of Arctic permafrost soil carbon under the GeoMIP
705 G6solar and G6sulfur experiments. Earth System Dynamics, 14(1), 39–53. https://doi.org/10.5194/esd-14-
706 39-2023, 2023.
707 Liu, C., Li, W., Zhu, G., Zhou, H., Yan, H., and Xue, P.: Land use/land cover changes and their driving Factors in
708 the Northeastern Tibetan Plateau based on geographical detectors and Google Earth Engine: A case study
709 in Gannan Prefecture. Remote Sensing, 12(19), Article 19. https://doi.org/10.3390/rs12193139, 2020.
710 Liu, C., Frazier, P., & Kumar, L. Comparative assessment of the measures of thematic classification accuracy.
711 Remote Sensing of Environment, 107(4), 606–616. https://doi.org/10.1016/j.rse.2006.10.010, 2007.
712 Luo, Y., Zhu, Z., Zhao, W., Li, M., Chen, J., Zhao, P., Sun, L., Zhang, Y., Duanmu, Z., and Chen, J.: Hybrid global
713 annual 1-km IGBP land cover maps for the period 2000–2020. Journal of Remote Sensing, 4, 0122.
714 https://doi.org/10.34133/remotesensing.0122, 2024.
715 Mack, M. C., Walker, X. J., Johnstone, J. F., Alexander, H. D., Melvin, A. M., Jean, M., and Miller, S. N.: Carbon
716 loss from boreal forest wildfires offset by increased dominance of deciduous trees. Science, 372(6539),
717 280–283. https://doi.org/10.1126/science.abf3903, 2021.
718 Mahdavi, S., Salehi, B., Granger, J., Amani, M., Brisco, B., & Huang, W. Remote sensing for wetland classification:
719 A comprehensive review. GIScience & Remote Sensing, 55(5), 623–658.
720 https://doi.org/10.1080/15481603.2017.1419602, 2018.
721 Mahdianpari, M., Salehi, B., Mohammadimanesh, F., Brisco, B., Homayouni, S., Gill, E., DeLancey, E. R., and

https://doi.org/10.5194/essd-2026-29
Preprint. Discussion started: 7 April 2026

Bourgeau-Chavez, L.: Big data for a big country: The first generation of Canadian wetland inventory map at a spatial resolution of 10-m using Sentinel-1 and Sentinel-2 data on the google earth engine cloud computing platform. Canadian Journal of Remote Sensing, 46(1), 15–33. https://doi.org/10.1080/07038992.2019.1711366, 2020.

Maxwell, A. E., Strager, M. P., Warner, T. A., Ramezan, C. A., Morgan, A. N., and Pauley, C. E.: Large-area, high spatial resolution land cover mapping using Random Forests, GEOBIA, and NAIP orthophotography: findings and recommendations. Remote Sensing, 11(12), Article 12. https://doi.org/10.3390/rs11121409, 2019.

Melvin, A. M., Mack, M. C., Johnstone, J. F., David McGuire, A., Genet, H., and Schuur, E. A. G.: Differences in ecosystem carbon distribution and nutrient cycling linked to forest tree species composition in a mid-successional Boreal forest. Ecosystems, 18(8), 1472–1488. https://doi.org/10.1007/s10021-015-9912-7, 2015.

Miller, P. A., and Smith, B.: Modelling tundra vegetation response to recent Arctic warming. AMBIO, 41(3), 281–291. https://doi.org/10.1007/s13280-012-0306-1, 2012.

Myers-Smith, I. H., Forbes, B. C., Wilmking, M., Hallinger, M., Lantz, T., Blok, D., Tape, K. D., Macias-Fauria, M., Sass-Klaassen, U., Lévesque, E., Boudreau, S., Ropars, P., Hermanutz, L., Trant, A., Collier, L. S., Weijers, S., Rozema, J., Rayback, S. A., Schmidt, N. M., and Hik, D. S.: Shrub expansion in tundra ecosystems: Dynamics, impacts and research priorities. Environmental Research Letters, 6(4), 045509. https://doi.org/10.1088/1748-9326/6/4/045509, 2011.

Neigh, C. S. R., Nelson, R. F., Ranson, K. J., Margolis, H. A., Montesano, P. M., Sun, G., Kharuk, V., Næsset, E., Wulder, M. A., and Andersen, H.-E.: Taking stock of circumboreal forest carbon with ground measurements, airborne and spaceborne LiDAR. Remote Sensing of Environment, 137, 274–287. https://doi.org/10.1016/j.rse.2013.06.019, 2013.

Oehri, J., Schaepman-Strub, G., Kim, J.-S., Grysko, R., Kropp, H., Grünberg, I., Zemlianskii, V., Sonnentag, O., Euskirchen, E. S., Reji Chacko, M., Muscari, G., Blanken, P. D., Dean, J. F., Di Sarra, A., Harding, R. J., Sobota, I., Kutzbach, L., Plekhanova, E., Riihelä, A., and Boike, J., et al.: Vegetation type is an important predictor of the Arctic summer land surface energy budget, Nature Communications, 13, 6379, https://doi.org/10.1038/s41467-022-34049-3, 2022.

https://doi.org/10.5194/essd-2026-29
Preprint. Discussion started: 7 April 2026

750 Olefeldt, D., Hovemyr, M., Kuhn, M. A., Bastviken, D., Bohn, T. J., Connolly, J., et al.: The Boreal–Arctic Wetland
751 and Lake Dataset (BAWLD). Earth System Science Data, 13(11), 5127–5149. https://doi.org/10.5194/essd-
752 13-5127-2021, 2021.
753 Olofsson, P., Foody, G. M., Herold, M., Stehman, S. V., Woodcock, C. E., and Wulder, M. A.: Good practices for
754 estimating area and assessing accuracy of land change. Remote Sensing of Environment, 148, 42–57.
755 https://doi.org/10.1016/j.rse.2014.02.015, 2014.
756 Pan, Y., Birdsey, R. A., Phillips, O. L., Houghton, R. A., Fang, J., Kauppi, P. E., Keith, H., Kurz, W. A., Ito, A.,
757 Lewis, S. L., Nabuurs, G.-J., Shvidenko, A., Hashimoto, S., Lerink, B., Schepaschenko, D., Castanho, A.,
758 & Murdiyarso, D. The enduring world forest carbon sink. Nature, 631(8021), 563–569.
759 https://doi.org/10.1038/s41586-024-07602-x, 2024.
760 Pérez-Hoyos, A., García-Haro, F. J., and San-Miguel-Ayanz, J.: A methodology to generate a synergetic land-cover
761 map by fusion of different land-cover products. International Journal of Applied Earth Observation and
762 Geoinformation, 19, 72–87. https://doi.org/10.1016/j.jag.2012.04.011, 2012.
763 Poulter, B., MacBean, N., Hartley, A., Khlystova, I., Arino, O., Betts, R., Bontemps, S., Boettcher, M., Brockmann,
764 C., Defourny, P., Hagemann, S., Herold, M., Kirches, G., Lamarche, C., Lederer, D., Ottlé, C., Peters, M.,
765 and Peylin, P.: Plant functional type classification for earth system models: Results from the European
766 Space Agency's Land Cover Climate Change Initiative. Geoscientific Model Development, 8(7), 2315–
767 2328. https://doi.org/10.5194/gmd-8-2315-2015, 2015.
768 Prestele, R., Alexander, P., Rounsevell, M. D. A., Arneth, A., Calvin, K., Doelman, J., et al.: Hotspots of uncertainty
769 in land-use and land-cover change projections: A global-scale model comparison. Global Change Biology,
770 22(12), 3967–3983. https://doi.org/10.1111/gcb.13337, 2016.
771 Raynolds, M. K. and Walker, D. A.: Circumpolar relationships between permafrost characteristics, NDVI, and
772 Arctic vegetation types, in: Proceedings of the Ninth International Conference on Permafrost, Fairbanks,
773 Alaska, USA, 29 June–3 July 2008, Institute of Northern Engineering, University of Alaska Fairbanks,
774 1469–1474, 2008.
775 Rogan, J., and Chen, D.: Remote sensing technology for mapping and monitoring land-cover and land-use change.
776 Progress in Planning, 61(4), 301–325. https://doi.org/10.1016/S0305-9006(03)00066-7, 2004.
777 Rollins, M. G.: LANDFIRE: A nationally consistent vegetation, wildland fire, and fuel assessment. International

https://doi.org/10.5194/essd-2026-29
Preprint. Discussion started: 7 April 2026

778 Journal of Wildland Fire, 18(3), 235–249. https://doi.org/10.1071/WF08088, 2009.
779 Schuur, E. A. G., Abbott, B. W., Commane, R., Ernakovich, J., Euskirchen, E., Hugelius, G., et al.: Permafrost and
780 climate change: Carbon cycle feedbacks from the warming Arctic. Annual Review of Environment and
781 Resources, 47(Volume 47, 2022), 343–371. https://doi.org/10.1146/annurev-environ-012220-011847,
782 2022.
783 Stinson, G., Magnussen, S., Boudewyn, P., Eichel, F., Russo, G., Cranny, M., and Song, A.: Canada. In National
784 Forest Inventories (pp. 233–247). Springer, Cham. https://doi.org/10.1007/978-3-319-44015-6_12, 2016.
785 Tape, K., Sturm, M., and Racine, C.: The evidence for shrub expansion in northern Alaska and the Pan-Arctic.
786 Global Change Biology, 12(4), 686–702. https://doi.org/10.1111/j.1365-2486.2006.01128.x, 2006.
787 Thompson, C., Beringer, J., Iii, F. S. C., and McGuire, A. D.: Structural complexity and land-surface energy
788 exchange along a gradient from Arctic tundra to boreal forest. Journal of Vegetation Science, 15(3), 397–
789 406. https://doi.org/10.1111/j.1654-1103.2004.tb02277.x, 2004.
790 Treat, C. C., Marushchak, M. E., Voigt, C., Zhang, Y., Tan, Z., Zhuang, Q., Virtanen, T. A., Räsänen, A., Biasi, C.,
791 Hugelius, G., Kaverin, D., Miller, P. A., Stendel, M., Romanovsky, V., Rivkin, F., Martikainen, P. J., and
792 Shurpali, N. J.: Tundra landscape heterogeneity, not interannual variability, controls the decadal regional
793 carbon balance in the Western Russian Arctic. Global Change Biology, 24(11), 5188–5204.
794 https://doi.org/10.1111/gcb.14421, 2018.
795 Turetsky, M. R., Kotowska, A., Bubier, J., Dise, N. B., Crill, P., Hornibrook, E. R. C., Minkkinen, K., Moore, T. R.,
796 Myers-Smith, I. H., Nykänen, H., Olefeldt, D., Rinne, J., Saarnio, S., Shurpali, N., Tuittila, E.-S.,
797 Waddington, J. M., White, J. R., Wickland, K. P., and Wilmking, M.: A synthesis of methane emissions
798 from 71 northern, temperate, and subtropical wetlands. Global Change Biology, 20(7), 2183–2197.
799 https://doi.org/10.1111/gcb.12580, 2014.
800 USGCRP.: Second state of the carbon cycle report (pp. 1–470). U.S. Global Change Research Program,
801 Washington, DC. https://carbon2018.globalchange.govhttps://carbon2018.globalchange.gov/chapter/11,
802 2018.
803 Virkkala, A.-M., Rogers, B. M., Watts, J. D., Arndt, K. A., Potter, S., Wargowsky, I., Schuur, E. A. G., See, C. R.,
804 Mauritz, M., Boike, J., Bret-Harte, M. S., Burke, E. J., Burrell, A., Chae, N., Chatterjee, A., Chevallier, F.,
805 Christensen, T. R., Commane, R., Dolman, H., … Natali, S. M. (2025). Wildfires offset the increasing but

https://doi.org/10.5194/essd-2026-29
Preprint. Discussion started: 7 April 2026

spatially heterogeneous Arctic–boreal CO2 uptake. *Nature Climate Change*, *15*(2), 188–195. https://doi.org/10.1038/s41558-024-02234-5

Virkkala, A.-M., Aalto, J., Rogers, B. M., Tagesson, T., Treat, C. C., Natali, S. M., et al.: Statistical upscaling of ecosystem CO2 fluxes across the terrestrial tundra and boreal domain: Regional patterns and uncertainties. Global Change Biology, 27(17), 4040–4059. https://doi.org/10.1111/gcb.15659, 2021.

Virkkala, A.-M., Virtanen, T., Lehtonen, A., Rinne, J., and Luoto, M.: The current state of CO2 flux chamber studies in the Arctic tundra: A review. Progress in Physical Geography: Earth and Environment, 42(2), 162–184. https://doi.org/10.1177/0309133317745784, 2018.

Walker, D. A., Raynolds, M. K., Daniëls, F. J. A., Einarsson, E., Elvebakk, A., Gould, W. A., Katenin, A. E., Kholod, S. S., Markon, C. J., Melnikov, E. S., Moskalenko, N. G., Talbot, S. S., and Yurtsev, B. A.: The Circumpolar Arctic vegetation map, J. Veg. Sci., 16, 267–282, https://doi.org/10.1111/j.1654-1103.2005.tb02365.x, 2005.

Wang, F., Kroeger, K. D., Gonneea, M. E., Pohlman, J. W., and Tang, J.: Water salinity and inundation control soil carbon decomposition during salt marsh restoration: An incubation experiment. Ecology and Evolution, 9(4), 1911–1921. https://doi.org/10.1002/ece3.4884, 2019.

Wang, J. A., Sulla-Menashe, D., Woodcock, C. E., Sonnentag, O., Keeling, R. F., and Friedl, M. A.: Extensive land cover change across Arctic–Boreal Northwestern North America from disturbance and climate forcing. Global Change Biology, 26(2), 807–822. https://doi.org/10.1111/gcb.14804, 2020.

Wang, L., Arora, V. K., Bartlett, P., Chan, E., and Curasi, S. R.: Mapping of ESA's Climate Change Initiative land cover data to plant functional types for use in the CLASSIC land model. Biogeosciences, 20(12), 2265–2282. https://doi.org/10.5194/bg-20-2265-2023, 2023.

White, J. C., Wulder, M. A., Hobart, G. W., Luther, J. E., Hermosilla, T., Griffiths, P., Coops, N. C., Hall, R. J., Hostert, P., Dyk, A., and Guindon, L.: Pixel-based image compositing for large-area dense time series applications and science. Canadian Journal of Remote Sensing, 40(3), 192–212. https://doi.org/10.1080/07038992.2014.945827, 2014.

Yu, Z. C.: Northern peatland carbon stocks and dynamics: A review. Biogeosciences, 9(10), 4071–4085. https://doi.org/10.5194/bg-9-4071-2012, 2012.

Zhang, W., Miller, P. A., Smith, B., Wania, R., Koenigk, T., and Döscher, R.: Tundra shrubification and tree-line

https://doi.org/10.5194/essd-2026-29
Preprint. Discussion started: 7 April 2026

advance amplify Arctic climate warming: Results from an individual-based dynamic vegetation model. Environmental Research Letters, 8(3), 034023. https://doi.org/10.1088/1748-9326/8/3/034023, 2013.